BIOCHEMISTRY
including biophysical chemistry & molecular biology

ARTICLE

pubs.acs.org/biochemistry

Dioxygen Transmembrane Distributions and Partitioning Thermodynamics in Lipid Bilayers and Micelles

M. Sameer Al-Abdul-Wahid,[†] Ferenc Evanics,[†] and R. Scott Prosser*[,†,‡]

[†]Department of Chemistry, University of Toronto, UTM, 3359 Mississauga Rd., North Mississauga, Ontario, Canada L5L 1C6
[‡]Department of Biochemistry, University of Toronto, Toronto, Ontario, Canada M5S 1A8

ABSTRACT: Cellular respiration, mediated by the passive diffusion of oxygen across lipid membranes, is key to many basic cellular processes. In this work, we report the detailed distribution of oxygen across lipid bilayers and examine the thermodynamics of oxygen partitioning via NMR studies of lipids in a small unilamellar vesicle (SUV) morphology. Dissolved oxygen gives rise to paramagnetic chemical shift perturbations and relaxation rate enhancements, both of which report on local oxygen concentration. From SUVs containing the phospholipid *sn*-2-perdeuterio-1-myristelaidoyl, 2-myristoyl-*sn*-glycero-3-phosphocholine (MLMPC), an analogue of 1,2-dimyristoyl-*sn*-glycero-3-phosphocholine (DMPC), we deduced the complete trans-bilayer oxygen distribution by measuring ^{13}C paramagnetic chemical shifts perturbations for 18 different sites on MLMPC arising from oxygen at a partial pressure of 30 bar. The overall oxygen solubility at 45 °C spans a factor of 7 between the bulk water (23.7 mM) and the bilayer center (170 mM) and is lowest in the vicinity of the phosphocholine headgroup, suggesting that oxygen diffusion across the glycerol backbone should be the rate-limiting step in diffusion-mediated passive transport of oxygen across the lipid bilayer. Lowering of the temperature from 45 to 25 °C gave rise to a slight decrease of the oxygen solubility within the hydrocarbon interior of the membrane. An analysis of the temperature dependence of the oxygen solubility profile, as measured by ^{1}H paramagnetic relaxation rate enhancements, reveals that oxygen partitioning into the bilayer is entropically favored ($\Delta S° = 54 \pm 3$ J K^{-1} mol^{-1}) and must overcome an enthalpic barrier ($\Delta H° = 12.0 \pm 0.9$ kJ mol^{-1}).

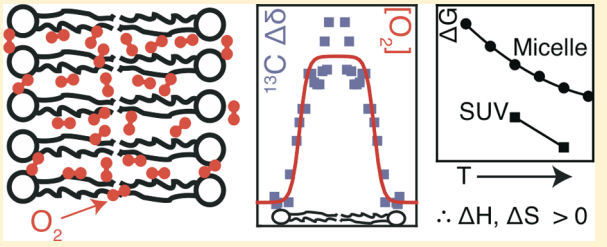

The distribution of oxygen in the cell and across its constituent membranes relates to a wide range of biochemical processes brought about by direct and indirect oxygen-sensing mechanisms.[1−8] For example, certain bacterial proteins make use of reversible redox states of reactive metals to serve as oxygen sensors. In mammals, hemoproteins function in carotid body type I cells as the primary oxygen sensing elements in the mitochondrial respiratory chain.[9] Others include a variety of potassium channel associated proteins, notably the plasma membrane associated protein, hemoxygenase-2, the prolyl hydroxylase family of enzymes, and the NAD(P)H oxidase enzymes which respond to reactive oxygen species.[9] Together, such sensing elements establish a sensitive network with which oxygen levels are vigilantly monitored. Even slight conditions of hypoxia trigger production of the transcription factor, HIF-1α, resulting in activation of as many as 70 genes.[10] The gene products mediate adaptive physiological responses including erythropoiesis, tissue vascularization, tumor development, and control of blood oxygen levels by the carotid and aortic bodies of the lung, heart, and vascular smooth muscle cells.[10] It is also likely that many multistep disulfide transfer reactions or oxidative folding steps in which the oxidizing capacity of molecular oxygen is utilized[11−13] must be positioned in membranes in such a way that the active site is situated in a region where oxygen is concentrated. Thus, details of the partitioning of oxygen in the cytoplasm, plasma membrane, and mitochondria of many cell types are crucial to our understanding of cell physiology.

This paper explores the detailed oxygen (O_2) distribution in phospholipid bilayers, from the perspective of solution state NMR using small unilamellar vesicles as the membrane model system. Paramagnetic shifts arising from O_2 and acting on ^{13}C nuclei in the phospholipids provide a detailed transmembrane profile of oxygen accessibility with atomic resolution, while paramagnetic $1/T_1$ rate enhancements (PREs) of ^{1}H nuclei at various temperatures provide information on the temperature dependence of oxygen solubility. Oxygen transport across lipid bilayers is not believed to be facilitated by channel proteins or active O_2 transporters. In this case, knowledge of the detailed transmembrane solubility profile, particularly in the vicinity of the glycerol backbone of the lipid headgroup where O_2 levels are lowest,[14] is relevant to the diffusion mediated transport of oxygen across membranes. The temperature dependence of the solubility profile can indicate if oxygen partitioning into the bilayers is driven by enthalpic or entropic considerations. Is trans-bilayer O_2 transport accomplished entirely by passive diffusion even in cells or organelles where large quantities of oxygen are either generated or utilized or might channel proteins or additional mechanisms be involved? To what extent does the degree of ordering of the bilayer, which may be affected by amphiphiles

Received: February 2, 2011
Revised: March 25, 2011
Published: March 26, 2011

such as cholesterol, affect oxygen solubility? The issue of the relative contribution of passive and facilitated diffusion is of direct consequence to our understanding of cell physiology.[15,16]

Current Methods of Detecting Oxygen Partitioning in Membranes. Our current understanding of the detailed partitioning of oxygen in membranes is derived from fluorescence[17−20] and electron spin resonance (ESR) studies[21−24] which rely on the quenching effect of oxygen on local fluorescent probes or spin−lattice relaxation enhancement on ESR spin-labels, while passive transport of oxygen across lipid monolayers deposited on a working electrode has been studied by electrochemical methods.[25−27] In both fluorescence and ESR, the measured effect of oxygen in the vicinity of the probe is the result of the diffusion-solubility product, $D_T[O_2]$, in the membrane, where D_T represents the local diffusion rate of oxygen. Extensive ESR measurements of the effects of oxygen in reconstituted lipid bilayers and native membranes have been carried out. These measurements generally make use of spin-labels attached to lipid-like amphiphiles or transmembrane peptides.[22,28] By performing a series of such measurements, in which the attached probe is confined to a range of immersion depths, an impression of the complete transmembrane accessibility of oxygen may be obtained.[22,24] The sensitivity of ESR and fluorescence permits extremely low probe molecule concentrations such that overall perturbations to lipid orientational order and dynamics are minimized. However, the possibility that the oxygen concentration or diffusivity near the probe is somehow disrupted cannot be discounted, making it difficult to ascertain the precise oxygen concentration and diffusivity profile in the membrane alone. Furthermore, it is difficult to reliably sample the diffusion−solubility product in the vicinity of the glycerol region of the phospholipid headgroup, where the introduction of a bulky probe critically perturbs local lipid packing and orientational order and thus the local oxygen diffusion−solubility product. Finally, quenching effects or ESR relaxation effects are significantly complicated by the fact that both D_T and $[O_2]$ vary with immersion depth.

NMR Approaches To Studying Oxygen Partitioning. ^{13}C NMR can also be used to assess local oxygen solubility in a lipid bilayer via O_2-induced paramagnetic shifts associated with ^{13}C lipid resonances.[14] There are several important distinctions between ESR or fluorescence and NMR in the interpretation of such effects from oxygen. First, the NMR approach requires no external probe molecule(s), and the paramagnetic effects are conveniently measured through chemical shift perturbations of the ^{13}C nuclear spin resonances. Second, if the ^{13}C resonances can be resolved, a single lipid may reveal the entire paramagnetic shift profile of the membrane, with angstrom resolution. Third, whereas ESR spin−lattice relaxation and fluorescence quenching effects depend on the diffusion−solubility product, $D_T[O_2]$, paramagnetic shifts from (unbound) oxygen, which are usually less than 100 Hz, fall in the weak collision limit and effectively depend only on the local concentration, $[O_2]$. Since the effects of O_2 through paramagnetic shifts are quite weak, relatively large partial pressures are required. Upon equilibration at an oxygen partial pressure of 30 bar, we observe distinct paramagnetic shifts between 0.1 and 1.0 ppm via ^{13}C NMR of the lipid constituents. To eliminate the overlap of methylene resonances typically observed in ^{13}C NMR spectra of saturated lipids such as DMPC, we make use of an unsaturated phospholipid, *sn*-2-perdeuterio-1-myristelaidoyl, 2-myristoyl-*sn*-glycero-3-phosphocholine (MLMPC). Deuteration of the *sn*-2 chain simplifies $[^1H,^{13}C]$ HSQC spectra, which show peaks only from the ^1H-bearing carbons in the *sn*-1 chain, glycerol backbone, and phosphocholine headgroup. The introduction of a *trans*-double bond between C9 and C10 of the *sn*-1 chain provides chemical shift dispersion of the methylene groups, such that all but a few methylene groups on the *sn*-1 chain of MLMPC are completely resolved in a $[^1H,^{13}C]$ HSQC NMR spectrum at 45 °C and a ^1H Larmor frequency of 600 MHz.[14]

To achieve the requisite resolution for solution state NMR studies of lipid bilayers, an isotropic bicelle model membrane system consisting of both MLMPC and short chain phospholipids may be used.[14] The combination of the two lipids is known to result in an aggregate consisting of an MLMPC-rich lipid bilayer whose hydrophobic edges are coated by a rim of short chain lipid.[29−33] By analyzing the paramagnetic shifts from oxygen along the entire length of the lipid in its bilayer state, the authors revealed a concentration profile of oxygen that spanned a factor of 10 from the headgroup to the hydrophobic interior. The results were corroborated by extensive molecular dynamics simulations of an oxygenated MLMPC lipid bilayer.[14] There are, however, potential shortcomings of the isotropic bicelle model membrane system associated with regard to the determination of the transmembrane oxygen accessibility profile. First, a significant proportion of the long chain phospholipids are expected to be in contact with the short chain lipids, which may also transiently partition into the phospholipid bilayer interior. This might lead to an average oxygen solubility profile that is not representative of that in a pure lipid bilayer. Second, it is difficult to obtain a broad temperature dependence of the oxygen solubility profile since MLMPC/DHPC demixing and bicelle size, which might influence the observed $[O_2]$ profile, are temperature-dependent.

To retain the small aggregate size required for solution state NMR studies, while most closely mimicking the natural lipid bilayer, we make use of small unilamellar vesicles (SUVs) composed of 95% MLMPC and 5% 1,2-dimyristoyl-*sn*-glycero-3-phospho-*rac*-1-glycerol (DMPG) to evaluate the detailed transmembrane oxygen solubility profile. Above the gel to liquid crystalline phase transition temperature, the negatively charged lipids are biologically relevant and render the vesicles colloidally stable for periods of several days, while the $[^1H,^{13}C]$ HSQC spectra provide excellent spectral resolution, as discussed below.

Paramagnetic effects of O_2 may be assessed in NMR experiments through either chemical shift perturbations (most commonly, ^{19}F and ^{13}C shifts) or through changes in spin−lattice (T_1) and spin−spin (T_2) relaxation times. Relaxation effects are most easily observed through ^1H or ^{19}F nuclei, whose large gyromagnetic ratios give rise to significant paramagnetic dipolar relaxation. A number of papers have focused on paramagnetic contributions to T_1 relaxation for purposes of studying protein topology or protein−protein interactions.[34−40] The expressions for T_1 relaxation from a freely diffusing paramagnet such as oxygen are well described[41,42] and depend sensitively on the so-called distance of closest approach between oxygen and the nuclear spin in addition to a geometric term associated with the local topology in the vicinity of the nucleus. Locally bound water and its associated exchange rate with bulk water significantly complicate the analysis in studies of protein topologies.[42] Moreover, in studies of membranes and solidlike networks, spin-diffusion effects may further compound the problem of obtaining a site-specific measure of oxygen accessibility via T_1.[43]

^{13}C NMR paramagnetic shifts from oxygen appear to reflect topology over a shorter length scale than that measured by spin−lattice relaxation from ^1H nuclei.[44] This can be seen from the significant variations in paramagnetic shifts even for nuclei in

a single residue in studies of protein topologies via [^{1}H,^{13}C] HSQC and ^{19}F NMR in the presence of dissolved oxygen.[45,46] Thus, in principle, ^{13}C paramagnetic shifts may provide a more precise profile of oxygen solubility across the membrane than that obtained by paramagnetic T_1 measurements of ^{1}H nuclei. Paramagnetic shifts from dissolved O_2 have been observed previously in studies of water-soluble proteins.[36,45] In one such study, the authors made use of ^{13}C paramagnetic shifts from dissolved oxygen to assess relative solvent exposure of backbone and side chain nuclei of a small soluble protein.[45] Residues that were clustered together exhibited a significant degree of protection from dissolved oxygen to the extent that completely solvent exposed and partly clustered residues of a natively unfolded protein could be easily distinguished based on paramagnetic shifts.[45]

MATERIALS AND METHODS

Sample Preparation. Dodecylphosphocholine (DPC) was obtained as a powder from Anatrace (Maumee, OH). DPC micelles were prepared in 50 mM pH 7 phosphate buffer to produce a 20% w/v dispersion. *sn*-2-perdeuterio-1-myristelaidoyl-2-myristoyl-*sn*-glycero-3-phosphocholine (MLMPC), and 1,2-dimyristoyl-*sn*-glycero-3-phospho-*rac*-1-glycerol (DMPG) were obtained as powders from Avanti Polar Lipids (Alabaster, AL). SUVs were prepared by first combining the dry lipids in an 19:1 ratio in 100 mM pH 7.04 HEPES buffer in D_2O to produce a 25% w/w dispersion. The dispersion was subsequently gently sonicated using a probe sonicator alternating between low-power sonication for 60 s and recovery in an ice bath for 120 s, for a total of 30 min. After sonication, samples were centrifuged for 30 s at 6000 rpm to remove bubbles and assess clarity and viscosity. After this procedure, samples were observed to be transparent or slightly birefringent and colloidally stable for as long as 8 days. This stability was a prerequisite for studies of oxygen permeation as a function of temperature, since 48 h was needed to equilibrate the sample with oxygen prior to NMR measurements, while 12 h was needed to equilibrate the sample upon changing the temperature.

NMR Experiments. All NMR experiments were performed on a 600 MHz Varian Inova spectrometer using a cryogenically cooled HCN liquids probe. In the case of oxygen paramagnetic rate measurements, the sample was pressurized in a 5 mm o.d. sapphire NMR tube (Saphikon, NH) to 50 bar oxygen partial pressure for 2 days to speed up equilibration rates and then equilibrated in the magnet overnight while maintaining the desired final pressure of 30 bar. Temperature-dependent measurements were performed in the direction of increasing temperature, since oxygen solubility in water is highest at lower temperatures. Contact shifts were obtained from [^{1}H,^{13}C] HSQC spectra with a substantial number of increments in the indirect dimension to provide sufficient resolution of peaks in the acyl chain region of MLMPC. PREs were obtained from ^{1}H T_1 spectra. Spectra were compared to those obtained under 30 bar He partial pressure to factor out any pressure-induced shifts (which in our experience are 0.1 ppm or less, data not shown) or changes in T_1 rates. Absolute referencing of the chemical shift was established through the Varian "setref" macro which establishes ^{13}C and ^{1}H chemical shifts based on the ^{2}H lock signal; identical transmitter frequencies were used in both the oxygenated and un-oxygenated samples in order to obtain an absolute change in chemical shift from oxygen. Typical ^{13}C and ^{1}H pulse lengths were 13.0 and 8 μs, respectively, while most [^{1}H,^{13}C] HSQC spectra were obtained using 16 scans, 512 increments, and a repetition time of either 2.5 or 1.5 s, for ambient or oxygenated membranes, respectively. A spectral width of 9900 Hz was used in the indirect (^{13}C) dimension such that the two vinyl ^{13}C resonances were folded into the spectrum. ^{1}H and ^{13}C chemical shift assignments were based on prior shift assignments.[14] Resonances arising from DMPG were distinguished from those of MLMPC by comparing peak intensities of [^{1}H,^{13}C] HSQC spectra from two samples whose MLMPC/DMPG ratios differed from 5:1 to 19:1 (data not shown). Data processing and spectral analysis were performed using NMRPipe[47] and NMRView.[48]

RESULTS AND DISCUSSION

The Paramagnetic Shift and Its Utility for Studies of Oxygen Partitioning. Figure 1 compares the assigned [^{1}H,^{13}C] HSQC spectra associated with MLMPC at 45 °C under ambient conditions (black) and at an oxygen partial pressure of 30 bar (red). The average SUV radius was determined to be 24 ± 2 nm at 45 °C based on pulsed field gradient-based diffusion measurements.[49] Although the SUV represents a larger model membrane system than the isotropic bicelle membrane model system used earlier,[14] MLMPC resonances are well resolved in the HSQC spectra. A cursory examination of the region of the spectrum associated with the *sn*-1 acyl chain of MLMPC reveals eight ^{13}C resonances with average ^{1}H and ^{13}C line widths on the order of 24 and 32 Hz, versus 25 and 18 Hz, respectively, for the former bicelle sample at equivalent temperatures.

Our approach in studies of the oxygen solubility profile in membranes has been to make use of paramagnetic shifts associated with ^{13}C nuclei, which may be most easily observed through a [^{1}H,^{13}C] HSQC. Oxygen-induced paramagnetic shifts have been used to study membrane immersion depth in ^{19}F NMR studies of membranes[50] and detergent solubilized membrane proteins.[51] Here, our focus is not on topology, but on the distribution of oxygen in the lipid bilayer. Note that the paramagnetic shifts exhibited in Figure 1 are observed in both the ^{13}C and the ^{1}H dimension and are accompanied by a modest amount of line broadening (1.5−39 Hz in the ^{13}C dimension and 1−32 Hz in the ^{1}H dimension) due in part to the relatively short electronic spin−lattice relaxation time of O_2.[52] Higher O_2 partial pressures give rise to paramagnetic shifts proportional to the pressure but at the expense of line broadening. Thus, the optimal partial pressure in a given experiment will depend on the desired resolution.

Interpreting Paramagnetic Shifts in Terms of the Transmembrane O_2 Solubility Profile. Assuming oxygen is freely and rapidly diffusing in the membrane, the paramagnetic shifts are of a contact nature, arising from unpaired electron spin density at the oxygen nuclei. In the weak collision limit and in the absence of oxygen binding, we expect the shift perturbation on the *i*th carbon nucleus, $\Delta\delta_i$, to be proportional to the local oxygen concentration, $[O_2]$, which in turn depends on bilayer immersion depth, z.[14] In a fluid lipid bilayer, each ^{13}C nucleus may undergo significant excursions of immersion depth, thereby sampling a range of O_2 concentrations. We therefore utilize an all-atom molecular dynamics (MD) simulations of oxygen and MLMPC in a hydrated lipid bilayer[14] to provide the MD-derived immersion depth distribution functions associated with the lipid ^{13}C nuclei, $\rho_i(z)$, and express the paramagnetic shift as[14]

$$\Delta\delta_i = k \int \rho_i(z)[O_2(z)]\, dz \qquad (1)$$

where k is a scaling factor and the integral accounts for the ensemble average. Note that the paramagnetic shifts associated with carbon

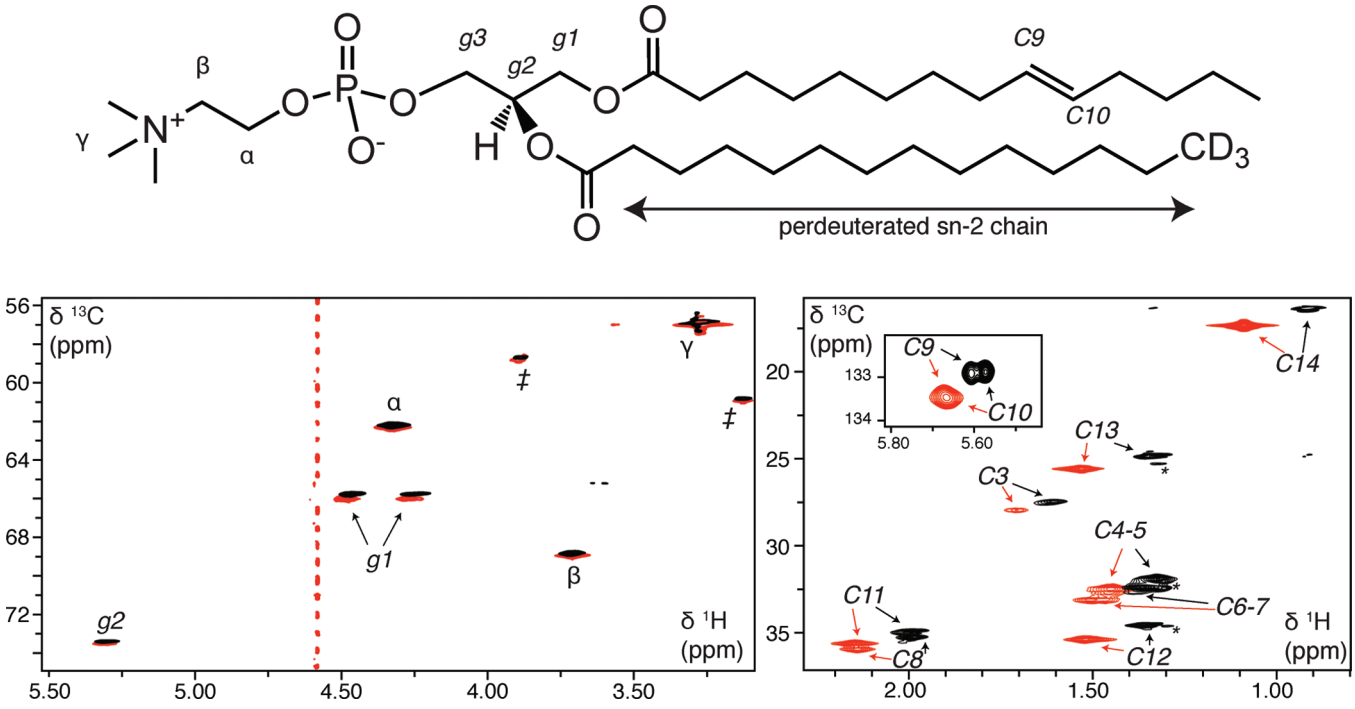

Figure 1. Assigned [^{1}H,^{13}C] HSQC spectra of MLMPC/DMPG (19:1 mole ratio) in a small unilamellar vesicle morphology. The structure of MLMPC is shown at the top of the figure for convenience. Spectra were acquired at 45 °C under diamagnetic conditions (He partial pressure of 30 bar, black) and paramagnetic conditions (O_2 partial pressure of 30 bar, red). The left panel shows peaks from the headgroup region, while the right panel peaks arising from the acyl chain. The olefinic region (right panel, inset) was collected in a separate experiment. The two *g1* protons are in different chemical shift environments and give rise to two peaks in the HSQC, while paramagnetic broadening of the residual water peak gives rise to the ridge at 4.6 ppm (^{1}H) in the spectrum collected under paramagnetic conditions. HEPES buffer peaks are marked with a double dagger (‡), while visible DMPG peaks are marked with an asterisk (∗).

sites in the double bond, $\Delta\delta_9$ and $\Delta\delta_{10}$, must be corrected by multiplying the raw paramagnetic shifts by 1.2 to account for differences in delocalization and polarizability associated with the sp^2-bonded carbon nuclei.[14]

While MD simulations provide an estimate of $[O_2(z)]$, there is lack of consensus on the diffusional accessibility of oxygen in lipid bilayers from the perspective of MD simulations.[24,53,54] We therefore restrict the use of the MD-derived $[O_2(z)]$ to providing an estimate of the scaling factor k, via a global nonlinear least-squares fit of the experimentally determined $\Delta\delta_i$ to the MD-derived $[O_2(z)]$ and $\rho_i(z)$ using eq 1.[14] From this fit we estimate the scaling factor k = 720 Hz $(mol/L)^{-1}$.

Modeling the Transmembrane O_2 Solubility Profile as a Boltzmann Sigmoid. Assuming oxygen partitioning is due to a difference in the chemical potential between that in water and the membrane interior,[22,23,28] $[O_2(z)]$ may be modeled as a Boltzmann sigmoid:

$$[O_2(z)] = ([O_2]^{water} - [O_2]^{max}) \left(\frac{1}{1+e^{(z-z_0)/\lambda}} - \frac{1}{1+e^{(z+z_0)/\lambda}}\right) + [O_2]^{water} \quad (2)$$

where oxygen concentrations range from a minimum, $[O_2]^{water}$, in bulk water ($|z|$ > 28 Å) to a maximum, $[O_2]^{max}$, in the hydrophobic bilayer center (z = 0 Å). $[O_2]^{water}$ is fixed to the known solubility of oxygen in 50 mM buffer.[55] z_0 designates an immersion depth where the oxygen gradient is greatest, while λ characterizes the effective width of the distribution function.

The fitted Boltzmann sigmoid parameters, $[O_2]^{max}$, z_0, and λ, are extracted from a global nonlinear least-squares fit of the experimentally determined $\Delta\delta_i$ using eq 1, where $[O_2(z)]$ is of the Boltzmann sigmoid form in eq 2. At a temperature of 45 °C and an O_2 partial pressure of 30 bar, oxygen concentrations were found to span a factor of 7 across the bilayer, ranging from $[O_2]^{water}$ = 23.7 mM to $[O_2]^{max}$ = 170 mM, while z_0 = 11.7 Å and λ = 1.27 Å. The fitted values are qualitatively similar to those estimated by ESR via site directed spin-labels on lipids and transmembrane peptides.[23,24,28] Since oxygen partitioning is so sensitive to local void volumes, the spin-label may introduce a subtle packing perturbation or local disorder which would give rise to higher local O_2 measurements in regions of the membrane where oxygen partitioning is otherwise unfavorable.

The validity of the fits of both the Boltzmann sigmoidal $[O_2(z)]$ and the scaling factor k is assessed by back-predicting paramagnetic shifts via eq 1. Figure 2 demonstrates the good agreement between the experimentally observed paramagnetic shifts (filled squares) and those back-predicted using the Boltzmann sigmoid $[O_2(z)]$ (hollow diamonds). The agreement between predicted and experimentally determined contact shifts is quite similar to a previous study of MLMPC in an isotropic bicelle.[14] While the SUV system does not provide the same level of resolution as isotropic bicelles, we note that the lipid headgroup (namely, the α, β, and g2 carbon nuclei), where close intermolecular packing via electrostatic and hydrogen bonding interactions gives rise to low void volume,[56−58] exhibits the lowest oxygen contact shifts and therefore the lowest local $[O_2]$ in the bilayer. Along the *sn*-1 chain, we observe a factor of 2.5 increase in paramagnetic shifts, from C2 to C14. This increase in local oxygen solubility correlates with the increasing disorder gradient of the lipid *sn*-1 acyl chain toward the methyl terminus.[59] Oxygen molecules occupy the "void volumes" generated by

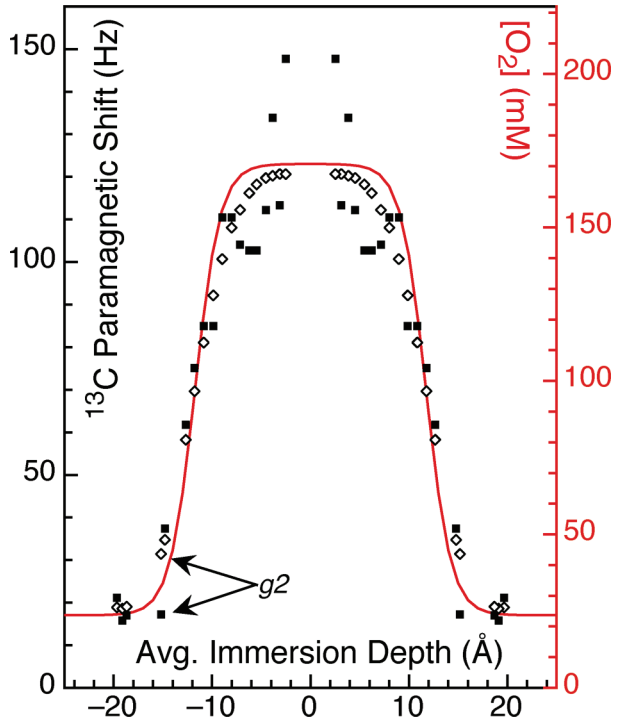

Figure 2. ^{13}C paramagnetic shifts (filled squares) of MLMPC in small unilamellar vesicles (i.e., MLMPC/DMPG mole ratio of 19:1) at 45 °C and an O_2 partial pressure of 30 bar, as a function of MD-derived average immersion depth of each site. The hydrophobic center of the lipid bilayer is defined by $z = 0$. The Boltzmann sigmoid $[O_2(z)]$, which spans a factor of 7 across the bilayer, is shown in red, with the corresponding $[O_2]$ scale on the right axis of the chart. Using this $[O_2(z)]$, a set of back-predicted paramagnetic shifts (hollow diamonds) was generated via eq 1. While the experimental and back-predicted shifts are generally in good agreement, a "dip" in the actual $[O_2]$ near the *g2* position cannot be reflected in the Boltzmann sigmoid $[O_2(z)]$, resulting in an 82% relative error in the back-predicted value at the *g2* position.

disorder in the acyl chain; as the number of voids increases toward the middle of the bilayer,[53] so does the local oxygen solubility.

Some fine details in the actual transmembrane O_2 solubility profile are not reflected in the Boltzmann sigmoid $[O_2(z)]$, which assumes the membrane interior and bulk water each have a constant chemical potential, without regard to molecular features. In particular, molecular dynamics simulations have shown that O_2 solubility in the region of the glycerol backbone is lower than that of water,[14] and the experimentally observed paramagnetic shift for the *g2* site in the glycerol backbone (Figure 2) also suggests a low $[O_2]$ near the glycerol backbone. The 82% error in the back-predicted value for the *g2* site is thus attributed to the Boltzmann sigmoid's inability to replicate this "dip" in O_2 solubility. Similarly, while the double bond at C9−C10 of the MLMPC lipid molecule is necessary to produce sufficient ^{13}C chemical shift dispersion to observe 10 distinct sites along the acyl chain, we observe paramagnetic shifts that do not correspond well to the Boltzmann sigmoid in this region, likely due to the difference associated with local disorder around the double bond.

Oxygen Thermodynamics in Small Unilamellar Vesicles. The MLMPC/DMPG bilayer exists in a fluid phase between 25 and 45 °C. Although gas solubility in liquids is inversely proportional to temperature, the opposite trend is observed in lipid bilayers, which is presumably a direct consequence of the well-known ordering in the acyl chains at lower temperatures. As the chains become more ordered, the population of voids or local defects is reduced, thereby lowering gas solubility. We express the equilibrium constant associated with oxygen partitioning from the aqueous phase to the membranous phase as the ratio of paramagnetic effects in the bilayer interior to those in water. For this purpose we resort to ^{1}H T_1 experiments where we simultaneously observe the effect of oxygen on the membrane interior and on water. Here, we define the equilibrium constant in terms of a ratio of paramagnetic relaxation enhancements (PREs) associated with the spin−lattice relaxation rate, $1/T_1$:

$$K_P = [O_2]^{max}/[O_2]^{water} \approx R_1^{para,interior}/R_1^{para,water} \quad (3)$$

where $R_1^{para,interior}$ is the PRE of the protons on the terminal methyl group of the *sn*-1 acyl chain of MLMPC and $R_1^{para,water}$ is the PRE of protons in bulk water. Using this equilibrium constant, we obtain the free energy of partitioning from the well-known expression

$$\Delta G = RT \ln K_P \quad (4)$$

where R represents the gas constant. Via this method, we estimate the free energy of oxygen partitioning in the lipid bilayer to be -4.0 ± 0.2 and -5.1 ± 0.1 kJ mol^{-1} at 25 and 45 °C, respectively. This is in excellent agreement with the free energy of oxygen partitioning obtained from the Boltzmann sigmoid $[O_2(z)]$ profile obtained from paramagnetic contact shift data at 45 °C (-5.2 kJ mol^{-1}). These values are comparable to free energies associated with partitioning of oxygen between oil and aqueous phases (-3.7 kJ mol^{-1})[60] and later computational estimates involving oxygen partitioning in lipid bilayers (-4.5 kJ mol^{-1}).[53]

The temperature dependence of the paramagnetic effects are also useful in terms of understanding the partitioning of oxygen into membranes. In particular, we ask if primarily enthalpic or entropic effects drive oxygen partitioning from water into membranes. Assuming the standard enthalpy of oxygen partitioning, $\Delta H°$, can be approximated as constant over the temperature range of interest, the van't Hoff equation provides both the enthalpic and entropic contributions to the free energy via the following well-known expressions

$$\ln\left(\frac{K_2}{K_1}\right) = \frac{\Delta H°}{R}\left(\frac{1}{T_2} - \frac{1}{T_1}\right) \quad (5)$$

$$\ln K_P = -\frac{\Delta H°}{RT} + \frac{\Delta S°}{R} \quad (6)$$

where K_2 and K_1 designate the equilibrium constants at temperatures T_2 and T_1, respectively. From this analysis we find that $\Delta H° = 12.0 \pm 0.9$ kJ mol^{-1} and $\Delta S° = 54 \pm 3$ J K^{-1} mol^{-1}, confirming that oxygen partitioning from water to the lipid bilayer is strongly entropically driven and must overcome an enthalpic barrier.

Oxygen Thermodynamics in Detergent Micelles. While both detergent micelles and bilayers have a hydrophobic center and hydrophilic exteriors, individual detergent molecules occupy a conical volume in a micelle, as compared to the roughly cylindrical volume occupied by individual lipids in an SUV. Does the difference in conical versus cylindrical packing affect oxygen partitioning? If so, is the difference a result of enthalpic or entropic differences between micelle and SUV? From ^{1}H PREs of DPC micelles, the free energy associated with oxygen partitioning is calculated to be -2.13 ± 0.04 and -2.95 ± 0.03 kJ mol^{-1} at 25

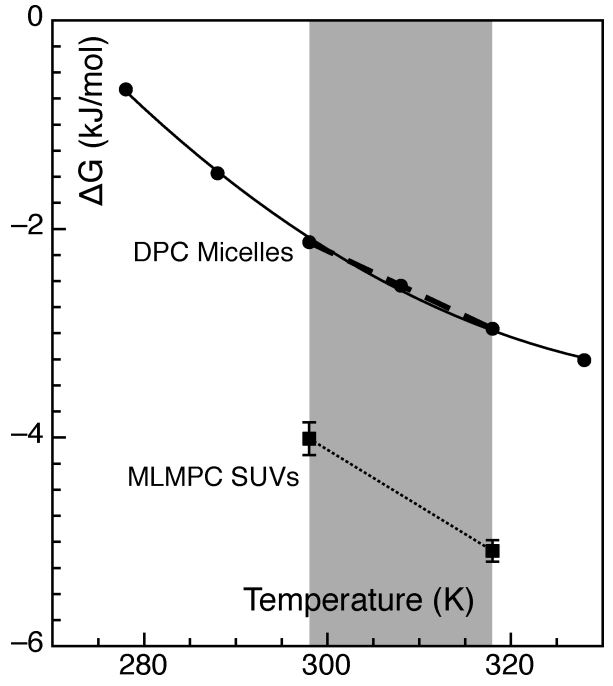

Figure 3. Change in Gibbs free energy (ΔG) upon transfer of oxygen into small unilamellar vesicles (i.e., MLMPC/DMPG mole ratio of 19:1, squares) and into DPC micelles (circles). Error bars for ΔG in DPC micelles are shorter than the height of the point. The shaded region represents the temperatures used in the determination of $\Delta H°$ and $\Delta S°$ via van't Hoff analysis of the free energy of partitioning in MLMPC SUVs (dotted line) and DPC micelles (dashed line), while the curved solid line represents the best fit of the free energy of O_2 partitioning in DPC micelles to eq 7, which determines $\Delta H°$ and $\Delta S°$ assuming a nonzero ΔC_p.

and 45 °C, respectively (Figure 3), indicating the oxygen solubility gradient is less pronounced in micelles as compared to lipid bilayers. Invocation of the van't Hoff equation over the ΔG values in this temperature region produces $\Delta H° = 10.2 \pm 0.2$ kJ mol^{-1} and $\Delta S° = 41.5 \pm 0.6$ J K^{-1} mol^{-1}. As with lipid bilayers, partitioning from water to the lipid bilayer is strongly entropically driven. From the perspective of oxygen solubility, the entropy associated with bilayer partitioning appears to be roughly ~30% greater than that of the micelle in the temperature range 25−45 °C. One temptation is to attribute this decrease in $\Delta S°$ to a difference in the degree of order of acyl chains in detergent micelles as compared to lipid bilayers. A convenient, quantitative measure of acyl chain order is the C−H bond order parameter, S_{CH}, which ranges from a value of −0.5 for an *all-trans* ordered chain to a value of 0 for a random mixture of *trans* and *gauche* conformers.[61] In both lipid bilayers[61−63] and detergent micelles,[64,65] experimentally determined S_{CH} values average around −0.2 for methylene groups in the acyl chain, dropping to almost zero at the methyl terminus. A molecular dynamics comparison of DPC micelles and 1,2-dipalmitoyl-*sn*-glycero-3-phosphocholine (DPPC) bilayers also suggests the degree of acyl chain ordering is similar in both systems.[66] We therefore speculate that the accessible free volume distribution,[53] which effectively describes the ratio of oxygen-accessible "voids" to total volume, is also the same for both micelle and bilayer. Because detergents in a micelle occupy a conical volume, the cross-sectional area per detergent molecule, and therefore the number of accessible voids, decreases toward to the center of the micelle as compared to their lipid counterparts, which occupy a cylindrical volume. This decrease in the number of available voids toward the center of the micelle may account for the oxygen solubility gradient being less pronounced in micelles as compared to lipid bilayers.

Even with the addition of 5% DMPG as a stabilizing agent, samples of MLMPC/DMPG SUVs were observed to be stable for no more than 8 days. Because of the time requirements of oxygen equilibration, measurements of oxygen solubility can be performed at up to three temperatures before the sample is no longer stable. DPC micelles, on the other hand, enjoy long-term sample stability, allowing measurement of ΔG at as many temperatures as desired. ΔG values for oxygen partitioning into DPC micelles over the temperature range of 5−55 °C are shown in Figure 3. The nonlinear temperature dependence of ΔG may arise from the change in the heat capacity (ΔC_p) of the system upon transfer of O_2 from the water into the micelle. If we assume ΔC_p to be independent of temperature, $\Delta H°$, $\Delta S°$, and ΔC_p are obtained from the nonlinear least-squares fit of ΔG values versus absolute temperate (T_{ref}) using the following equation:[67]

$$\Delta G = \Delta H° + \Delta C_p(T_{obs} - T_{ref}) - T_{obs}[\Delta S° + \Delta C_p \ln(T_{obs}/T_{ref})] \quad (7)$$

where we have used $T_{ref} = 298$ K. Via this method, we obtain $\Delta H° = 15.0 \pm 0.1$ kJ mol^{-1}, $\Delta S° = 57.2 \pm 0.1$ J K^{-1}, and $\Delta C_p = -0.37 \pm 0.01$ kJ K^{-1} mol^{-1} (Figure 3, solid line). While we refrain from comparing these thermodynamics values directly to those obtained via the van't Hoff equation, as the inclusion of the change of heat capacity substantially impacts the calculated enthalpy of partitioning, we note that the conclusions remain that partitioning is dictated by entropy.

CONCLUSIONS AND FINAL REMARKS

This study reports the oxygen distribution in a lipid bilayer via ^{13}C paramagnetic shifts, and the temperature dependence and thermodynamics of oxygen solubility via ^{1}H paramagnetic relaxation enhancements. Excellent spectral resolution is achieved using a membrane model system consisting of a colloidally stable mixture of MLMPC and DMPG. This suggests that the MLMPC/DMPG SUV should serve as a suitable membrane model system for the investigation of lipid bilayers and the study of the interaction of drugs and membrane additives by NMR, owing to its superior resolution and relative stability.

The focus in this paper was to ascertain the complete partitioning profile of oxygen in a lipid bilayer and determine if partitioning is enthalpically or entropically driven. Measurement of ^{13}C paramagnetic shifts from oxygen reveals the oxygen solubility profile spans a factor of 7 across the lipid bilayer, and oxygen concentrations are lowest in the vicinity of the lipid headgroup and glycerol backbone. The rate-limiting step in trans-bilayer oxygen permeation should arise from the barrier associated with low local oxygen solubility, low void volumes, and low oxygen diffusion rates[53] in this region of the bilayer. Given the significant range of the oxygen solubility across the bilayer, we speculate that membrane−protein complexes in which molecular oxygen is utilized in oxidative folding may well be positioned in regions of local disorder established either by the membrane or by residues in the vicinity of the active site, while the opposite should be true when oxygen inhibits a given enzymatic process. From ^{1}H PREs observed in the temperature range 25−45 °C, a van't Hoff analysis of the oxygen solubility in MLMPC/DMPG SUVs indicates that partitioning of oxygen from water to the

membrane interior is strongly entropically driven and must overcome an enthalpic barrier.

A comparison of oxygen partitioning in the MLMPC/DMPG SUV with that in DPC micelles reveals that the micelle system is slightly less disordered from the perspective of oxygen partitioning. We speculate this is due to the intrinsic nature of the micelle in which, unlike lipid bilayers, the conical volume occupied by each detergent molecule requires that the volume (and therefore the oxygen-accessible volume) decrease toward to the micelle center. While the observed ΔG values appear to be linear in the 25−45 °C region, measurement of ΔG values in the expanded region of 5−55 °C shows ΔG does not vary linearly with temperature. Correcting for the change in the heat capacity of the system results in a negative value for ΔC_p.

The intercalation and penetration of anesthetics such as short chain alcohols into the cell membrane is believed to affect key ion channels and/or neurotransmitter receptors either directly[68−74] and/or indirectly by altering physical properties of the membrane.[75−77] Although physiological levels of ethanol have relatively minor effects on lipid orientational order or dynamics, a transient interaction between ethanol and the glycerol lipid headgroup has been observed by NMR where the bound state lifetime is on the order of a few nanoseconds.[76,78] It is therefore tempting to hypothesize that passive diffusion of oxygen through the glycerol headgroup region of the bilayer serves as the rate-limiting step in overall trans-bilayer oxygen transport, and the addition of small amounts of permeabilizers such as DMSO or pentanol might alter lipid packing in this region and thus oxygen transport. This might in turn give rise to a multitude of downstream events associated with oxygen homeostasis.

MD Simulations. Note that MD simulations of carbon atom distributions and O_2 distributions were performed and described in detail in an earlier paper,[14] and the results of this lipid bilayer simulation were used directly for the analysis of oxygen paramagnetic shift data in the current SUV membrane model system.

AUTHOR INFORMATION

Corresponding Author

*E-mail: scott.prosser@utoronto.ca. Tel (905)-828-3802. Fax (905)-828-5425.

Funding Sources

R.S.P. acknowledges the Natural Sciences and Engineering Research Council of Canada (NSERC) and the Government of the Province of Ontario for financial support through the NSERC Discovery and Provincial Research Excellence Award (PREA) programs.

ACKNOWLEDGMENT

The authors thank Professor Robert Bryant (University of Virginia) for many helpful discussions.

ABBREVIATIONS

DMPG, 1,2-dimyristoyl-*sn*-glycero-3-phospho-*rac*-1-glycerol; DPC, dodecylphosphocholine; DPPC, 1,2-dipalmitoyl-*sn*-glycero-3-phosphocholine; ESR, electron spin resonance; HSQC, heteronuclear single quantum correlation; MLMPC, *sn*-2-perdeuterio-1-myristelaidoyl-2-myristoyl-*sn*-glycero-3-phosphocholine; PRE, paramagnetic relaxation enhancement; SUV, small unilamellar vesicle.

REFERENCES

(1) Prabhakar, N. R. (2001) Physiological and genomic consequences of intermittent hypoxia - Invited review: Oxygen sensing during intermittent hypoxia: cellular and molecular mechanisms. *J. Appl. Physiol. 90*, 1986–1994.

(2) Haddad, J. J. (2002) Oxygen-sensing mechanisms and the regulation of redox-responsive transcription factors in development and pathophysiology. *Respir. Res. 3*, xxx.

(3) Fandrey, J. (2004) Oxygen-dependent and tissue-specific regulation of erythropoietin gene expression. *Am. J. Physiol. 286*, R977–R988.

(4) Giaccia, A. J., Simon, M. C., and Johnson, R. (2004) The biology of hypoxia: the role of oxygen sensing in development, normal function, and disease. *Genes Dev. 18*, 2183–2194.

(5) Wolin, M. S., Ahmad, M., and Gupte, S. A. (2005) Oxidant and redox signaling in vascular oxygen sensing mechanisms: basic concepts, current controversies, and potential importance of cytosolic NADPH. *Am. J. Physiol. 289*, L159–L173.

(6) Weir, E. K., Lopez-Barneo, J., Buckler, K. J., and Archer, S. L. (2005) Mechanisms of disease - Acute oxygen-sensing mechanisms. *N. Engl. J. Med. 353*, 2042–2055.

(7) Acker, T., Fandrey, J., and Acker, H. (2006) The good, the bad and the ugly in oxygen-sensing: ROS, cytochromes and prolyl-hydroxylases. *Cardiovasc. Res. 71*, 195–207.

(8) Stockmann, C., and Fandrey, J. (2006) Hypoxia-induced erythropoietin production: A paradigm for oxygen-regulated gene expression. *Clin. Exp. Pharmacol. Physiol. 33*, 968–979.

(9) Lahiri, S., Roy, A., Baby, S. M., Hoshi, T., Semenza, G. L., and Prabhakar, N. R. (2006) Oxygen sensing in the body. *Prog. Biophys. Mol. Biol. 91*, 249–286.

(10) Semenza, G. L. (2003) Targeting HIF-1 for cancer therapy. *Nat. Rev. Cancer 3*, 721–732.

(11) Sevier, C. S., and Kaiser, C. A. (2006) Conservation and diversity of the cellular disulfide bond formation pathways. *Antioxid. Redox Signaling 8*, 797–811.

(12) Sevier, C. S., and Kaiser, C. A. (2008) Ero1 and redox homeostasis in the endoplasmic reticulum. *Biochim. Biophys. Acta, Mol. Cell Res. 1783*, 549–556.

(13) Sevier, C. S., and Kaiser, C. A. (2002) Formation and transfer of disulphide bonds in living cells. *Nat. Rev. Mol. Cell Biol. 3*, 836–847.

(14) Al-Abdul-Wahid, M. S., Yu, C. H., Batruch, I., Evanics, F., Pomes, R., and Prosser, R. S. (2006) A combined NMR and molecular dynamics study of the transmembrane solubility and diffusion rate profile of dioxygen in lipid bilayers. *Biochemistry 45*, 10719–10728.

(15) Hu, H. P., and Wu, M. X. (2001) Mechanism of anesthetic action: oxygen pathway perturbation hypothesis. *Med. Hypotheses 57*, 619–627.

(16) Talley, E. M., Sirois, J. E., Lei, Q. B., and Bayliss, D. A. (2003) Two-pore-domain (KCNK) potassium channels: Dynamic roles in neuronal function. *Neuroscientist 9*, 46–56.

(17) Chalpin, D. B., and Kleinfeld, A. M. (1983) Interaction of Fluorescence Quenchers with the Normal-(9-Anthroyloxy) Fatty-Acid Membrane Probes. *Biochim. Biophys. Acta 731*, 465–474.

(18) Dumas, D., Muller, S., Gouin, F., Baros, F., Viriot, M. L., and Stoltz, J. F. (1997) Membrane fluidity and oxygen diffusion in cholesterol-enriched erythrocyte membrane. *Arch. Biochem. Biophys. 341*, 34–39.

(19) Bronshtein, I., Afri, M., Weitman, H., Frimer, A. A., Smith, K. M., and Ehrenberg, B. (2004) Porphyrin depth in lipid bilayers as determined by iodide and parallax fluorescence quenching methods and its effect on photosensitizing efficiency. *Biophys. J. 87*, 1155–1164.

(20) Moller, M., Botti, H., Batthyany, C., Rubbo, H., Radi, R., and Denicola, A. (2005) Direct measurement of nitric oxide and oxygen partitioning into liposomes and low density lipoprotein. *J. Biol. Chem. 280*, 8850–8854.

(21) Windrem, D. A., and Plachy, W. Z. (1980) The Diffusion-Solubility of Oxygen in Lipid Bilayers. *Biochim. Biophys. Acta 600*, 655–665.

(22) Dzikovski, B. G., Livshits, V. A., and Marsh, D. (2003) Oxygen permeation profile in lipid membranes: Comparison with transmembrane polarity profile. *Biophys. J. 85*, 1005–1012.

(23) Marsh, D., Dzikovski, B. G., and Livshits, V. A. (2006) Oxygen profiles in membranes. *Biophys. J. 90*, L49–L51.
(24) Nielsen, R. D., Che, K. P., Gelb, M. H., and Robinson, B. H. (2005) A ruler for determining the position of proteins in membranes. *J. Am. Chem. Soc. 127*, 6430–6442.
(25) Ivanov, I. I., Fedorov, G. E., Gus'kova, R. A., Ivanov, K. I., and Rubin, A. B. (2004) Permeability of lipid membranes to dioxygen. *Biochem. Biophys. Res. Commun. 322*, 746–750.
(26) Borden, M. A., and Longo, M. L. (2004) Oxygen permeability of fully condensed lipid monolayers. *J. Phys. Chem. B 108*, 6009–6016.
(27) Pu, G., Longo, M. L., and Borden, M. A. (2005) Effect of microstructure on molecular oxygen permeation through condensed phospholipid monolayers. *J. Am. Chem. Soc. 127*, 6524–6525.
(28) Marsh, D. (2001) Polarity and permeation profiles in lipid membranes. *Proc. Natl. Acad. Sci. U.S.A. 98*, 7777–7782.
(29) Vold, R. R., Prosser, R. S., and Deese, A. J. (1997) Isotropic solutions of phospholipid bicelles: A new membrane mimetic for high-resolution NMR studies of polypeptides. *J. Biomol. NMR 9*, 329–335.
(30) Luchette, P. A., Vetman, T. N., Prosser, R. S., Hancock, R. E. W., Nieh, M. P., Glinka, C. J., Krueger, S., and Katsaras, J. (2001) Morphology of fast-tumbling bicelles: a small angle neutron scattering and NMR study. *Biochim. Biophys. Acta, Biomembr. 1513*, 83–94.
(31) Andersson, A., and Maler, L. (2005) Magnetic resonance investigations of lipid motion in isotropic bicelles. *Langmuir 21*, 7702–7709.
(32) Marcotte, I., and Auger, M. (2005) Bicelles as model membranes for solid- and solution-state NMR studies of membrane peptides and proteins. *Concepts Magn. Reson., Part A 24A*, 17–37.
(33) Prosser, R. S., Evanics, F., Kitevski, J. L., and Al-Abdul-Wahid, M. S. (2006) Current applications of bicelles in NMR studies of membrane-associated amphiphiles and proteins. *Biochemistry 45*, 8453–8465.
(34) Teng, C. L., and Bryant, R. G. (2000) Experimental measurement of nonuniform dioxygen accessibility to ribonuclease a surface and interior. *J. Am. Chem. Soc. 122*, 2667–2668.
(35) Hernandez, G., Teng, C. L., Bryant, R. G., and LeMaster, D. M. (2002) O-2 penetration and proton burial depth in proteins: Applicability to fold family recognition. *J. Am. Chem. Soc. 124*, 4463–4472.
(36) Ulmer, T. S., Campbell, I. D., and Boyd, J. (2002) The effects of dissolved oxygen upon amide proton relaxation and chemical shift in a perdeuterated protein. *J. Magn. Reson. 157*, 181–189.
(37) Ulmer, T. S., Ramirez, B. E., Delaglio, F., and Bax, A. (2003) Evaluation of backbone proton positions and dynamics in a small protein by liquid crystal NMR spectroscopy. *J. Am. Chem. Soc. 125*, 9179–9191.
(38) Teng, C. L., and Bryant, R. G. (2004) Mapping oxygen accessibility to ribonuclease a using high-resolution NMR relaxation spectroscopy. *Biophys. J. 86*, 1713–1725.
(39) Ellena, J. F., Moulthrop, J., Wu, J., Rauch, M., Jaysinghne, S., Castle, J. D., and Cafiso, D. S. (2004) Membrane position of a basic aromatic peptide that sequesters phosphatidylinositol 4,5 bisphosphate determined by site-directed spin labeling and high-resolution NMR. *Biophys. J. 87*, 3221–3233.
(40) Sakakura, M., Noba, S., Luchette, P. A., Shimada, I., and Prosser, R. S. (2005) An NMR method for the determination of protein-binding interfaces using dioxygen-induced spin-lattice relaxation enhancement. *J. Am. Chem. Soc. 127*, 5826–5832.
(41) Freed, J. H. (1978) Dynamic Effects of Pair Correlation-Functions on Spin Relaxation by Translational Diffusion in Liquids 0.2. Finite Jumps and Independent T1 Processes. *J. Chem. Phys. 68*, 4034–4037.
(42) Teng, C. L., Hinderliter, B., and Bryant, R. G. (2006) Oxygen accessibility to ribonuclease A: Quantitative interpretation of nuclear spin relaxation induced by a freely diffusing paramagnet. *J. Phys. Chem. A 110*, 580–588.
(43) Huster, D., and Gawrisch, K. (1999) NOESY NMR crosspeaks between lipid headgroups and hydrocarbon chains: Spin diffusion or molecular disorder? *J. Am. Chem. Soc. 121*, 1992–1993.
(44) Li, X., Rinkevicius, Z., Tu, Y., Tian, H., and Ögren, H. (2009) Paramagnetic Perturbation of the 19F NMR Chemical Shift in Fluorinated Cysteine by O2: A Theoretical Study, *The Journal of Physical Chemistry B 113*, 10916–10922.
(45) Bezsonova, I., Evanics, F., Marsh, J. A., Forman-Kay, J. D., and Prosser, R. S. (2007) Oxygen as a paramagnetic probe of clustering and solvent exposure in folded and unfolded states of an SH3 domain. *J. Am. Chem. Soc. 129*, 1826–1835.
(46) Evanics, F., Bezsonova, I., Marsh, J., Kitevski, J. L., Forman-Kay, J. D., and Prosser, R. S. (2006) Tryptophan solvent exposure in folded and unfolded states of an SH3 domain by F-19 and H-1 NMR. *Biochemistry 45*, 14120–14128.
(47) Delaglio, F., Grzesiek, S., Vuister, G. W., Zhu, G., Pfeifer, J., and Bax, A. (1995) Nmrpipe - a Multidimensional Spectral Processing System Based on Unix Pipes. *J. Biomol. NMR 6*, 277–293.
(48) Johnson, B. A., and Blevins, R. A. (1994) Nmr View - a Computer-Program for the Visualization and Analysis of Nmr Data. *J. Biomol. NMR 4*, 603–614.
(49) Al-Abdul-Wahid, M. S., Prosser, R. S. (2009) Unpublished results.
(50) Prosser, R. S., Luchette, P. A., and Westerman, P. W. (2000) Using O-2 to probe membrane immersion depth by F-19 NMR. *Proc. Natl. Acad. Sci. U.S.A. 97*, 9967–9971.
(51) Luchette, P. A., Prosser, R. S., and Sanders, C. R. (2002) Oxygen as a paramagnetic probe of membrane protein structure by cysteine mutagenesis and F-19 NMR spectroscopy. *J. Am. Chem. Soc. 124*, 1778–1781.
(52) Teng, C. L., Hong, H., Kiihne, S., and Bryant, R. G. (2001) Molecular oxygen spin-lattice relaxation in solutions measured by proton magnetic relaxation dispersion. *J. Magn. Reson. 148*, 31–34.
(53) Marrink, S. J., and Berendsen, H. J. C. (1996) Permeation process of small molecules across lipid membranes studied by molecular dynamics simulations. *J. Phys. Chem. 100*, 16729–16738.
(54) Shinoda, W., Mikami, M., Baba, T., and Hato, M. (2004) Molecular dynamics study on the effects of chain branching on the physical properties of lipid bilayers: 2. Permeability. *J. Phys. Chem. B 108*, 9346–9356.
(55) Weiss, R. (1970) The Solubility of Nitrogen, Oxygen and Argon in Water and Seawater. *Deep-Sea Res. 17*, 721–&.
(56) Marrink, S. J., Sok, R. M., and Berendsen, H. J. C. (1996) Free volume properties of a simulated lipid membrane. *J. Chem. Phys. 104*, 9090–9099.
(57) Seu, K. J., Cambrea, L. R., Everly, R. M., and Hovis, J. S. (2006) Influence of lipid chemistry on membrane fluidity: Tail and headgroup interactions. *Biophys. J. 91*, 3727–3735.
(58) Rabinovich, A. L., Balabaev, N. K., Alinchenko, M. G., Voloshin, V. P., Medvedev, N. N., and Jedlovszky, P. (2005) Computer simulation study of intermolecular voids in unsaturated phosphatidylcholine lipid bilayers. *J. Chem. Phys. 122*, xxxx.
(59) Dill, K. A., and Flory, P. J. (1981) Molecular-Organization in Micelles and Vesicles. *Proc. Natl. Acad. Sci. U.S.A. 78*, 676–680.
(60) Battino, R., Evans, F., and Danforth, W. (1968) The solubilities of seven gases in olive oil with references to theories of transport through the cell membrane. *J. Am. Oil Chem. Soc. 45*, 830–833.
(61) Seelig, J. (1977) Deuterium magnetic resonance: theory and application to lipid membranes. *Q. Rev. Biophys. 10*, 353–418.
(62) Aussenac, F., Laguerre, M., Schmitter, J. M., and Dufourc, E. J. (2003) Detailed structure and dynamics of bicelle phospholipids using selectively deuterated and perdeuterated labels. H-2 NMR and molecular mechanics study. *Langmuir 19*, 10468–10479.
(63) Salmon, A., Dodd, S. W., Williams, G. D., Beach, J. M., and Brown, M. F. (1987) Configurational statistics of acyl chains in polyunsaturated lipid bilayers from H-2 NMR. *J. Am. Chem. Soc. 109*, 2600–2609.
(64) Beswick, V., Guerois, R., Cordier-Ochsenbein, F., Coïc, Y.-M., Huynh-Dinh, T., Tostain, J., Noël, J.-P., Sanson, A., and Neumann, J.-M. (1998) Dodecylphosphocholine micelles as a membrane-like environment: New results from NMR relaxation and paramagnetic relaxation enhancement analysis. *Eur. Biophys. J. 28*, 48–58.
(65) Söderman, O., Walderhaug, H., Henriksson, U., and Stilbs, P. (1985) NMR relaxation in isotropic surfactant systems. A 2H, 13C, and 14N

NMR study of the micellar (L1) and cubic (I1) phases in the dodecyltrimethylammonium chloride/water system. *J. Phys. Chem. 89*, 3693–3701.

(66) Tieleman, D., van der Spoel, D., and Berendsen, H. (2000) Molecular dynamics simulations of dodecylphosphocholine micelles at three different aggregate sizes: Micellar structure and chain relaxation. *J. Phys. Chem. B 104*, 6380–6388.

(67) Baldwin, R. L. (1986) Temperature-Dependence of the Hydrophobic Interaction in Protein Folding. *Proc. Natl. Acad. Sci. U.S.A. 83*, 8069–8072.

(68) Mihic, S. J., Ye, Q., Wick, M. J., Koltchine, V. V., Krasowski, M. A., Finn, S. E., Mascia, M. P., Valenzuela, C. F., Hanson, K. K., Greenblatt, E. P., Harris, R. A., and Harrison, N. L. (1997) Sites of alcohol and volatile anaesthetic action on GABA(A) and glycine receptors. *Nature 389*, 385–389.

(69) Solt, K., Johansson, J. S., and Raines, D. E. (2006) Kinetics of anesthetic-induced conformational transitions in a four-alpha-helix bundle protein. *Biochemistry 45*, 1435–1441.

(70) Franks, N. P. (2006) Molecular targets underlying general anaesthesia. *Br. J. Pharmacol. 147*, S72–S81.

(71) Nagele, P., Mendel, J. B., Placzek, W. J., Scott, B. A., d'Avignon, D. A., and Crowder, M. (2005) Volatile anesthetics bind rat synaptic snare proteins. *Anesthesiology 103*, 768–778.

(72) Lobo, I. A., and Harris, R. A. (2005) Sites of alcohol and volatile anesthetic action on glycine receptors. *Int. Rev. Neurobiol. 65*, 53.

(73) Hemmings, H. C., Akabas, M. H., Goldstein, P. A., Trudell, J. R., Orser, B. A., and Harrison, N. L. (2005) Emerging molecular mechanisms of general anesthetic action. *Trends Pharmacol. Sci. 26*, 503–510.

(74) Slater, S. J., Malinowski, S. A., and Stubbs, C. D. (2004) The nature of the hydrophobic n-alkanol binding site within the C1 domains of protein kinase C alpha. *Biochemistry 43*, 7601–7609.

(75) Carnini, A., Phillips, H., Shamrakov, L., and Cramb, D. (2004) Revisiting lipid - general anesthetic interactions (II): Halothane location and changes in lipid bilayer microenvironment monitored by fluorescence. *Can. J. Chem. 82*, 1139–1149.

(76) Feller, S. E., Brown, C. A., Nizza, D. T., and Gawrisch, K. (2002) Nuclear overhauser enhancement spectroscopy cross-relaxation rates and ethanol distribution across membranes. *Biophys. J. 82*, 1396–1404.

(77) Ly, H. V., and Longo, M. L. (2004) The influence of short-chain alcohols on interfacial tension, mechanical properties, area/molecule, and permeability of fluid lipid bilayers. *Biophys. J. 87*, 1013–1033.

(78) Koenig, B. W., and Gawrisch, K. (2005) Lipid-ethanol interaction studied by NMR on bicelles. *J. Phys. Chem. B 109*, 7540–7547.